



Fluorescent iridium nanoclusters for selective determination of chromium(VI)

Malin Cui¹ · Chan Wang² · Dapeng Yang¹ · Qijun Song²

Received: 30 July 2017 / Accepted: 9 November 2017 / Published online: 2 December 2017
© Springer-Verlag GmbH Austria, part of Springer Nature 2017

Abstract

Fluorescent iridium nanoclusters (IrNCs) consisting of up to 7 Ir atoms were prepared by heating IrCl₃ in N,N-dimethylformamide. No other reagents are required. High resolution transmission electron microscopy (HRTEM) shows the IrNCs to be monodispersed with an average size of 0.9 ± 0.2 nm. They are well soluble in polar solvents and stable in these solvents for at least 6 months. Under photoexcitation with 365 nm light, they emit strong bluish green fluorescence with peaks that depend on the excitation wavelength and range from 530 to 650 nm. The fluorescence lifetime typically is 2.2 ns and the quantum yield is 8.3%. Fluorescence is quenched by Cr(VI) ion (chromate), and the emission peak is gradually red-shifted. According to the absorbance spectra of IrNCs in the presence and absence of Cr(VI) and Stern-Volmer quenching behavior study, static quenching is involved. Based on these findings, a selective assay was developed for the determination of Cr(VI). It has a linear response in the 0.1 to 100 μM chromate concentration range and a 25 nM detection limit.

Keywords IrNCs · Fluorescence · N,N-dimethylformamide · Cr(VI) · Static quenching · Red-shift · Ligand-to-metal charge transfer · Electron-rich atoms · Excitation wavelength-dependent emission

Introduction

The unique optical, electric, magnetic and catalytic properties of noble metal nanoclusters have attracted broad interests in recent years [1]. Compared with the larger noble metal nanoparticles, they consist of a few atoms and exhibit unique molecular-like behavior, including HOMO-LUMO transitions, optical chirality, quantized charging, discrete electronic states, absorbance and fluorescence features [2]. They have offered potential applications in bioimaging [3], photonics [4], sensing [5] and catalysis [6]. The noble metal nanoclusters of Au NCs [7], Ag NCs [8] and Pt NCs [1] have been

extensively exploited, including their preparations, properties and their potential applications. Stable self-assembled gold particles were prepared using a cationic polymer to cross-link fluorescent Au NCs by Guével et al. [3]. They showed a 4-fold fluorescence enhancement due to the aggregation-induced emission phenomenon (AIE), and can be used to multimodal cellular imaging, multiple drug/biomolecule loading and releasing, which will be highly interesting for application in theranostics. Near-infrared-emitting protoporphyrin IX-linked gold clusters (PFL-AuC) were synthesized and used for the selective fluorescence imaging assisted photodynamic therapy (PDT) [4]. The accurate localization of the PFL-AuC on tumor cells and effective generation of singlet oxygen induced by the PFL-AuC facilitated targeted cell death. The NIR emission of the PFL-AuC was also beneficial to the real-time tracking of the PDT. These works promote the further development of fluorescent noble metal nanoclusters-based photonics therapeutic agent for clinical practice.

In contrast to Au, Ag and Pt nanomaterials, the Ir nanomaterials were mainly explored for their catalytic applications [9], very few attempts have been made in the study of fluorescent IrNCs. So far only three papers presented the preparation of such IrNCs [10, 11]. The non-fluorescent Ir NPs are prepared under the reducing action of NaBH₄, and then fluorescent IrNCs were formed by adding 2,2'-binaphthol. The

Malin Cui and Chan Wang contributed equally to this work.

Electronic supplementary material The online version of this article (<https://doi.org/10.1007/s00604-017-2553-0>) contains supplementary material, which is available to authorized users.

✉ Qijun Song
qsong@jiangnan.edu.cn

¹ College of Chemical Engineering & Materials Science, Quanzhou Normal University, Quanzhou 362000, China

² The Key Laboratory of Food Colloids and Biotechnology, Ministry of Education, School of Chemical and Material Engineering, Jiangnan University, Wuxi 214122, China

preparation process needed 2 days to complete in toluene media, which is quite toxic, complicated and time-consuming. The monolayer protected IrNCs were synthesized via a solid state method [11]. Precursor IrCl_3 , stabilizer 2-phenylethanethiol and reductant NaBH_4 are mixed and grinded to prepare IrNCs, which are extracted in toluene. The synthetic strategy is simple, although the fluorescence is much weaker than other noble metal nanoclusters, and the toxic organic solvent is used. Obora et al. prepared the DMF-stabilized IrNCs with blue emission in mixture medium of water and DMF [12]. This IrNCs can be used as a catalyst in the β -methylation of alcohols using methanol as the C1 source. However, the detailed discussions on formation mechanism and optical properties of IrNCs have not been provided. Thus, it is still a challenging task to prepare bright fluorescent IrNCs through a green approach.

In this work, the bluish green fluorescent IrNCs were prepared in DMF solution without addition of any other reagents. According to matrix-assisted laser desorption ionization time-of-flight mass spectrometry (MALDI-TOF MS) investigation results, the IrNCs consisted of 2 to 7 Ir atoms. They possessed different emissions in water, ethanol and DMF, and the emission spectra typically depended upon the excitation wavelength. The emission can be sensitively and selectively quenched by Cr(VI), due to the formation of the non-fluorescent ground-state complex between IrNCs and Cr(VI). Hence a fluorescent method based on the IrNCs was developed for the determination of Cr(VI) in water.

Materials and methods

Materials and instruments

Iridium (III) chloride trihydrate ($\text{IrCl}_3 \cdot 3\text{H}_2\text{O}$) was purchased from Aladdin Industrial Co., Ltd. (Shanghai, China, <http://www.chemcd.com/supplier/aladdin.html>). DMF, EtOH, potassium phosphate (K_3PO_4), potassium hydrogen phosphate anhydrous (K_2HPO_4), potassium phosphate monobasic (KH_2PO_4), phosphoric acid (H_3PO_4), sodium chloride (NaCl), potassium chloride (KCl), magnesium sulphate (MgSO_4), barium chloride (BaCl_2), lithium chloride (LiCl), zinc nitrate hexahydrate ($\text{Zn}(\text{NO}_3)_2 \cdot 6\text{H}_2\text{O}$), aluminium sulfate ($\text{Al}_2(\text{SO}_4)_3$), manganese (II) sulfate tetrahydrate ($\text{MnSO}_4 \cdot 4\text{H}_2\text{O}$), cobaltous chloride hexahydrate ($\text{CoCl}_2 \cdot 6\text{H}_2\text{O}$), strontium nitrate ($\text{Sr}(\text{NO}_3)_2$), nickel sulfate hexahydrate ($\text{NiSO}_4 \cdot 6\text{H}_2\text{O}$), lead nitrate ($\text{Pb}(\text{NO}_3)_2$), cupric chloride (CuCl_2), ferrous sulfate (FeSO_4), ferric chloride (FeCl_3), mercury (II) chloride (HgCl_2) and cadmium chloride (CdCl_2) were purchased from Sinopharm Chemical Reagent Co., Ltd. (Shanghai, China, <http://www.sangon.com/product>). All reagents were of analytical grade and were used without

further purification. Milli-Q ultrapure water (18.2 $\text{M}\Omega \cdot \text{cm}$) was used throughout all experiments.

The fluorescence spectra analysis was carried out on a fluorescence spectrophotometer (Edinburgh Instruments, <https://www.edinst.com/products/fs5-spectrofluorometer/>) with a 1.0 cm quartz cell (Ex slit 5 nm, Em slit 5 nm). The fluorescence lifetime of the IrNCs was measured using steady state fluorescence lifetime spectrometers (FLS 980-STM, Edinburgh Instruments, <https://www.photonics.com/Product.aspx?PRID=59994>). Absorbance spectra of the IrNCs were carried out on a UV-vis spectrophotometer (UV-2700, Japan Shimadzu Co., Ltd., http://www.shimadzu.com/an/molecular_spectro/uv/uv2600_2700.html) with a 1 cm quartz cuvette. Matrix-assisted laser desorption ionization time-of-flight mass spectrometry (MALDI-TOF MS) (ultrafleXtreme, Bruker Corporation, <https://www.bruker.com/products/mass-spectrometry-and-separations/maldi-toftof/new-ultraflextreme/overview.html>) measurement of the IrNCs was performed using 2-[(2E)-3-(4-tert-butylphenyl)-2-methylprop-2-enylidene] malononitrile (DCTB) as a matrix. The structure of the IrNCs was analyzed by Fourier transform infrared spectrometer (FTIR, WQF-600 N, <https://www.china.cn/guangpuyi/3657535594.html>). Phase identification of the IrNCs were conducted with X-ray diffraction (XRD, D8, Bruker AXS Co., Ltd., <http://www.vincent.org.rs/en/equipment/xrd-diffractometer-bruker-axs-d8-bruker-germany/>) using $\text{Cu-K}\alpha$ radiation source ($\lambda = 1.54051 \text{ \AA}$) over the 2θ range of $3\text{--}90^\circ$. The oxidation state of iridium was analyzed by X-ray photoelectron spectroscopy (XPS) using a PHI Quantum 2000 Scanning ESCA Microprobe (<http://www.phl.com/surface-analysis-techniques/xps-esca.html>). High resolution transmission electron microscopy (HRTEM, FEI Tecnai 30, Holland FEI Corporation, <http://engineering.case.edu/centers/scsam/microscopes/transmission-electron/technai>) was performed at 300 kV to visualize the prepared IrNCs, and energy dispersive X-ray (EDX) analysis of the IrNCs was carried out. The sample for TEM measurement was prepared by slow evaporation of the IrNCs ethanol solution on a carbon film supported by 300-mesh Cu grids. The Zeta potential of IrNCs was determined by using the Zeta potential analyzer (Brookhaven instruments Corporation, <https://www.brookhaveninstruments.com/nanobrook-zetapals-potential-analyzer>).

Synthesis of the fluorescent IrNCs

IrCl_3 (0.0179 g) was added to 20 mL DMF and dissolved under ultrasound. The reddish brown IrCl_3 solution was refluxed in 140°C under vigorous stirring for 1 h, the color of the solution changed to faint yellow and the weak blue fluorescence was observed. After the continuously stirring for 9 h, yellowish-brown fluorescent IrNCs formed. The excess solvent was vacuum evaporated below 76 mmHg at

90 °C for 1 h and the residue was redissolved in appropriate solvent for use.

Quantum yield calculation of the IrNCs

The fluorescence quantum yield (Φ) [13, 14] of the IrNCs was calculated by using quinine sulfate ($\Phi = 0.54$, dissolved in 0.1 M H₂SO₄) as the standard sample [15]. To minimize the self-absorption effect, the IrNCs and the quinine sulfate solution were prepared with their absorbance less than 0.05 at the excitation wavelength of the IrNCs. The Φ of the IrNCs can be acquired according to equation $\Phi_x = \Phi_s \times \frac{F_x}{F_s} \times \frac{A_s}{A_x} \times \frac{n_s^2}{n_x^2}$, where the subscripts *s* and *x* denote the standard and the sample test, respectively. *F* stands for the integrated fluorescence intensity, *A* represents absorbance and η is the refractive index of the solvent.

Determination of Cr(VI)

The fluorescent IrNCs were used for the determination of Cr(VI) in pH 3.0 acetate buffer. Different Cr(VI) concentrations were added into the 0.5 mM IrNCs solution under room temperature. Due to the excitation and emission wavelengths of IrNCs red-shifted with increasing of Cr(VI) concentration, thus the excitation wavelength corresponding to the maximum fluorescence intensity was used according to the Cr(VI) concentration. The fluorescence intensities of the blank solution (IrNCs) and the test solution (IrNCs-Cr(VI)) were recorded and labelled with F_0 and F_1 , respectively. The fluorescence intensity difference $\Delta F (= F_0 - F_1)$ was also obtained, which was directly related to the concentration of Cr(VI). A regression equation was then established and it was used to evaluate the sensitivity of this method. The selectivity was also estimated by recording the fluorescence responses of IrNCs in the presence of other interferences.

Sample analysis

Different water samples from tap water, lake and seawater were analyzed to determine the Cr(VI) content based on the fluorescent IrNCs. According to reference [16], these water samples were purified by filtration with 0.22 μ m Millipore filter to remove large solids. 1.00 mL fresh water samples were taken and complexed with 1.00 mL 4.0 mM EDTA. The mixture was centrifuged at 8000 g for 20 min. Spiked samples were prepared by adding 100 μ L of 5 mM, 3 mM and 2 mM Cr(VI) into 900 μ L supernatant liquid and then were added into 4.00 mL 0.625 mM Ir NCs including pH 3.0 acetate buffer. The fluorescence intensity was recorded and the concentration of Cr(VI) calculated according to the regression equation.

Results and discussion

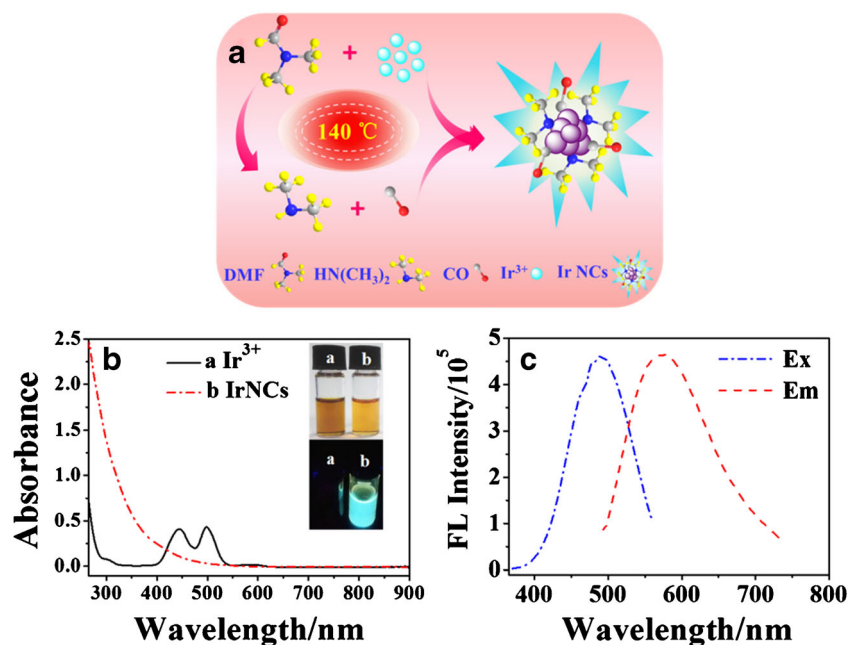
Choice of materials

DMF was chosen as the solvent and stabilizer for the preparation of IrNCs. Firstly, it can be decomposed into CO and dimethylamine under high temperature, which are electron donor and π -acid ligand, respectively [17]. CO and dimethylamine can react with Ir³⁺ to form complex and is reduced to generate IrNCs. Regarding to AuNPs and AgNPs, they can earlier react with the macromolecules such as hyperbranched poly(amidoamine) [18], poly(diallyl dimethylammonium) chloride [19]. DMF is more economical stabilizer for the preparation of IrNCs than biomolecules. Secondly, due to the difference of electric structure, the stability of Ir is much higher than Au and Ag, thus IrNCs is much suitable for practical application. Thirdly, the AuNPs were used for the determination of Cr(VI) via colorimetric assay. Molecular-like IrNCs possesses higher sensitivity than AuNPs in the analysis of Cr(VI) [20].

Preparation and characterization of the IrNCs

The IrNCs were prepared in DMF solution without using any other reagents. Under 140 °C and in the presence of Ir³⁺, the DMF was decomposed into CO and dimethylamine with reducibility [17], which can adsorb on the surface of Ir³⁺ and reduced Ir³⁺ to Ir(0). With the gradually increasing of Ir(0), few Ir atoms stacked into molecular-like IrNCs (Fig. 1a). The preparation conditions, including Ir³⁺ concentration, reaction temperature and time, have a great influence on the formation of the IrNCs (Fig. S1). With the increasing of Ir³⁺ concentration, the fluorescence spectra of the IrNCs red-shift and the fluorescence intensity enhances gradually. While the Ir³⁺ concentration is over 3 mM, the excessive growth of the IrNCs will lead to the decline of fluorescence intensity (Fig. S1A). Increasing reaction temperature to 140 °C, the fluorescence intensity reaches the maximum and it will decline with the consecutive increasing of reaction temperature. This is related closely to the decomposition rate of DMF. Too slow decomposition will postpone the formation of the IrNCs, while rapid decomposition will decrease the reduction efficiency of Ir³⁺ (Fig. S1C). Thus, under 140 °C, 3 mM Ir³⁺ was incubated for 10 h to prepare the fluorescent IrNCs. Too long reaction time will also lead to the over growth of the IrNCs and decrease the fluorescence intensity (Fig. S1E). The photographs of the IrNCs under visible and 365 nm UV light were accord with the fluorescence spectra of the IrNCs under corresponding reaction conditions (Fig. S1B, D, F). The quantum yield of IrNCs was calculated to be 8.3% using quinine sulfate as reference [13, 15].

Fig. 1 **a** Schematic illustration of the IrNC preparation; **b** the UV-vis absorbance spectra of Ir³⁺ and IrNCs, inset: the corresponding photographs of Ir³⁺ and fluorescent IrNCs under visible light and 365 nm UV light; **c** the fluorescence spectra of IrNCs



The Ir³⁺ solution has three obvious absorbance peaks at 301, 443 and 498 nm. With the formation of the fluorescence IrNCs, the three peaks disappeared completely, suggesting that all Ir³⁺ were involved in the preparation of IrNCs (Fig. 1b). The brownish red IrNCs emit strong bluish green fluorescence under 365 nm UV light (inset of Fig. 1b), and show the maximum excitation and emission wavelength at 487 and 575 nm, respectively (Fig. 1c).

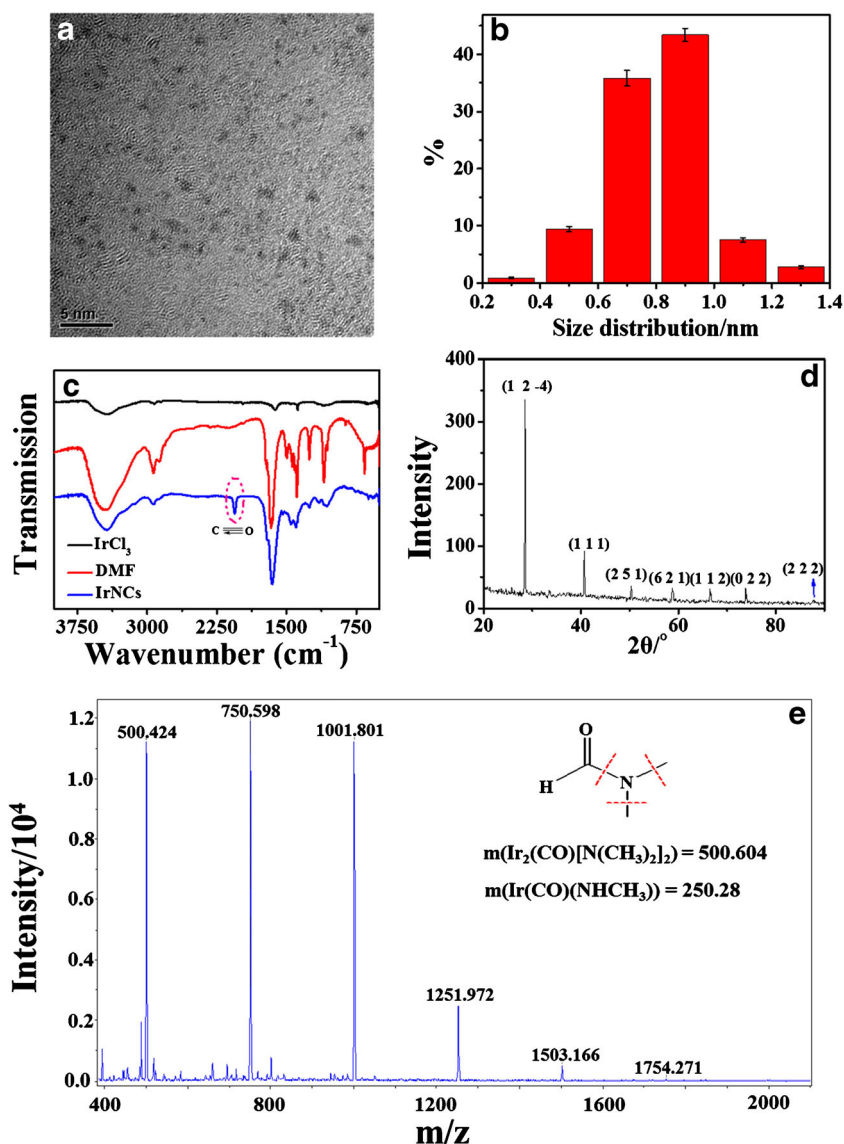
The IrNCs exhibit fairly uniformity and good monodispersity, the average diameter is about ca. 0.9 ± 0.2 nm based on the statistic result of 76 particles (Fig. 2a, b). FTIR spectra were used to further evidence the chemical structure of the IrNCs (Fig. 2c). IrCl₃ has no obvious FTIR absorbance peaks but three weak peaks at 3435, 1621 and 1382 cm⁻¹. Compared with DMF, there is a new peak appearance at 2060 cm⁻¹ in the FTIR spectrum of IrNCs, which attribute to the adsorption of CO on the surface of IrNCs [21, 22]. These results suggest DMF is decomposed to form CO and dimethylamine with reducibility, which can reduce Ir³⁺ to form the fluorescent IrNCs. XRD pattern of the IrNCs shows the diffraction peaks observed at 2θ values of 28.3, 40.7, 50.3, 58.8, 66.5, 73.9 and 88 correspond to (12-4), (111), (251), (621), (112), (022) and (222) facets of the IrNCs (Fig. 2d). Facets of (251) and (621) are assigned to Ir₄(CO)₁₂, indicating CO is adsorbed on the surface of the IrNCs. Facets of (111) and (222) are contributed to the Ir crystals, suggesting Ir(0) is present throughout the IrNCs. MALDI-TOF MS spectrum demonstrated the existence of sub-nanometer-sized IrNCs containing 2 to 7 Ir atoms. The masses of the dominant molecular ions at 500.424, 750.598, 1001.801, 1251.972, 1503.166 and 1754.271 are in accordance with Ir₂(CO)[N(CH₃)₂]₂, Ir₃(CO)₂[N(CH₃)₂]₂(NHCH₃), Ir₄(CO)₃[N(CH₃)₂]₂(NHCH₃)₂,

Ir₅(CO)₄[N(CH₃)₂]₂(NHCH₃)₃, Ir₆(CO)₅[N(CH₃)₂]₂(NHCH₃)₄ and Ir₇(CO)₆[N(CH₃)₂]₂(NHCH₃)₅ (Fig. 2e). These results confirm the formation of IrNCs consisting of 2–7 Ir atoms by the reduction actions of CO and dimethylamine to Ir³⁺.

The XPS spectra of the IrNCs were used to identify the oxidation state of Ir and the interaction with N and O. The survey spectrum of the IrNCs shows four typical peaks of Ir 4f, N 1s, O 1s, C 1s and the corresponding content of each element were measured to be 1.16%, 14.06%, 12.79% and 71.98%, respectively (Fig. S2A). The high-resolution spectra of the Ir 4f regions reveal two chemical state: Ir(0) characterized by 4f7/2 and 4f5/2 with binding energies of 60.9 and 63.8 eV, respectively; and Ir^{δ+}-O/N of 61.8 and 64.5 eV (Fig. S2B) [23]. Two peaks of O 1s high-resolution spectra at 531.3 and 532.1 correspond to —C=O and Ir^{δ+}-O, respectively (Fig. S2C). The binding energies of N 1s at 399.7 and 400.7 eV indicate the presence of two relative nitrogen species of C-N-C and Ir^{δ+}-N, respectively (Fig. S2D) [24]. The high-resolution C1s spectra of the IrNCs revealed the presence of C-O (284.7 eV), C-N (285.8 eV) and —C=O (287.6 eV) (Fig. S2E). These results further confirm the interaction of Ir with CO and N in DMF, which are consistent with the results from FTIR.

The lifetime of the excited state is defined by the average time the molecule spends in the excited state prior to return to the ground state [13]. Fig. S3 shows the time-resolved fluorescence decay curve of the IrNCs and the fluorescence lifetime was calculated to be 2.2 ns (Table S1). The fluorescence spectra of the IrNCs are red-shifted upon the increasing of excitation wavelength (Fig. 3). This excitation wavelength-dependent emission can be

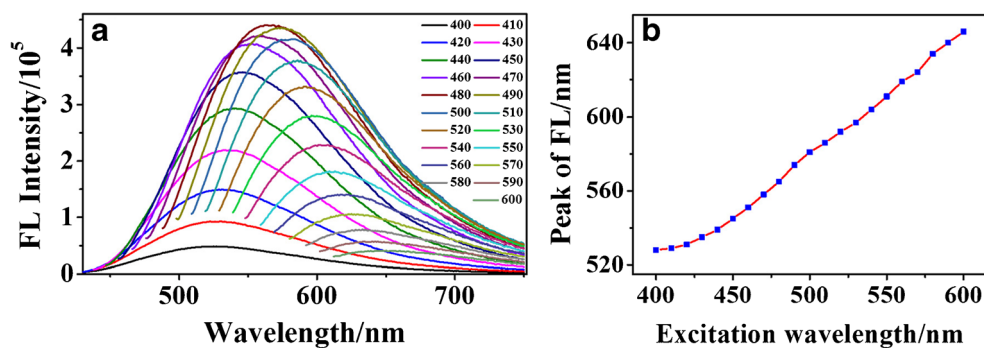
Fig. 2 **a** HRTEM of the IrNCs; **b** the particle diameter distribution of the IrNCs; **c** FTIR of IrCl₃, DMF and Ir NC; **d** XRD of the IrNCs; **e** MALDI mass spectrum of IrNCs in the positive ion mode



explained by spectral broadening mechanism [25]. DMF contains electron-rich atoms of nitrogen and oxygen and a fraction of electron is transferred to the Ir atoms of IrNCs to form ligand-to-metal charge transfer (LMCT) complexes [26]. IrNCs are stabilized by accepting and localizing the electron density, and extent of localization

determines the clusters size by preventing from the excessive growth and induces electronic asymmetry. Due to the high polarity of DMF, the LMCT will possess high dipole moments and can interact with surrounding dipoles. This action perturbs the energy of the ground state to some extent and thus site distributions form with different

Fig. 3 **a** Fluorescence emission spectra of the IrNCs at various excitation wavelengths; **b** the PL peak of the IrNCs as a function of excitation wavelength



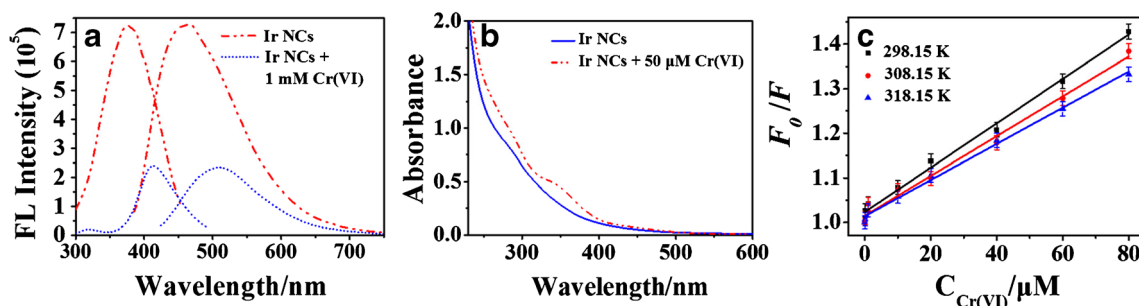


Fig. 4 **a** The fluorescence of (a) the IrNCs and (b) IrNCs + 1 mM Cr(VI), **b** UV-vis absorbance spectra of (c) IrNCs and (d) IrNCs + 50 μM Cr(VI), **c** Stern-Volmer plots of the fluorescence of IrNCs quenched by the Cr(VI)

under different reaction temperature. The F_0 and F values were obtained from the integrated emission intensity in the absence and presence of the Cr(VI), respectively

interaction energies. The ground-state heterogeneity contributes to monotonous shift of $\lambda_{\text{max}}^{\text{em}}$ as a function of λ_{ex} and $\lambda_{\text{max}}^{\text{ex}}$ as a function of λ_{em} in a manner [27].

The solvent polarity and the local environment have profound effects on the fluorescence spectra by the solvent-fluorophore interactions [13]. If the interaction occurs in the ground state, the some change in the excitation spectrum is expected. If the interaction only occurs in the excited state, the polar additive does not affect the excitation spectrum. As shown in **Fig. S4**, the excitation and emission spectra of the IrNCs in water ($\lambda_{\text{ex}} = 458$ nm, $\lambda_{\text{em}} = 542$ nm), EtOH ($\lambda_{\text{ex}} = 479$ nm, $\lambda_{\text{em}} = 564$ nm) and DMF ($\lambda_{\text{ex}} = 477$ nm, $\lambda_{\text{em}} = 560$ nm) are appreciably different, suggesting the interactions occur in the ground state. Owing to the $n-\pi^*$ transition of the IrNCs, the formation of hydrogen bond of solvents will considerably influence the fluorescence spectra of the IrNCs. With the increasing of hydrogen bond formation ability of solvents, the energy gap increases between the first excited singlet states and the ground state, and the fluorescence spectra of the IrNCs will shift to short wavelength. It should be stated, however, that the fluorescence spectra and intensity show no obvious change with the storage of these materials for 6 months suggesting that the IrNCs possess good stability in ambient conditions (**Fig. S4**).

The fluorescence spectra appear blue-shift with the decreasing of the IrNCs concentration, simultaneously, fluorescence intensity increases from 3 mM to 0.5 mM and decreases when the concentration is lower than 0.5 mM (**Fig. S5**). This phenomenon is closely related to the surface state of the IrNCs [28]. The FTIR spectra show that the IrNCs contain C=O and N-H, thus, the IrNCs can form intermolecular hydrogen bonds and contribute to extended conjugation in the structure of the IrNCs. With the decreasing of IrNCs concentration, the hydrogen bonds are destroyed by the surrounding solvent molecules and the conjugation structure lessens, accompanying with the blue shift of the fluorescence spectra. The fluorescence intensity increases with decreasing of IrNCs concentration

in the range of 3 to 0.5 mM, which is the self-quenching phenomenon of high concentration fluorophore.

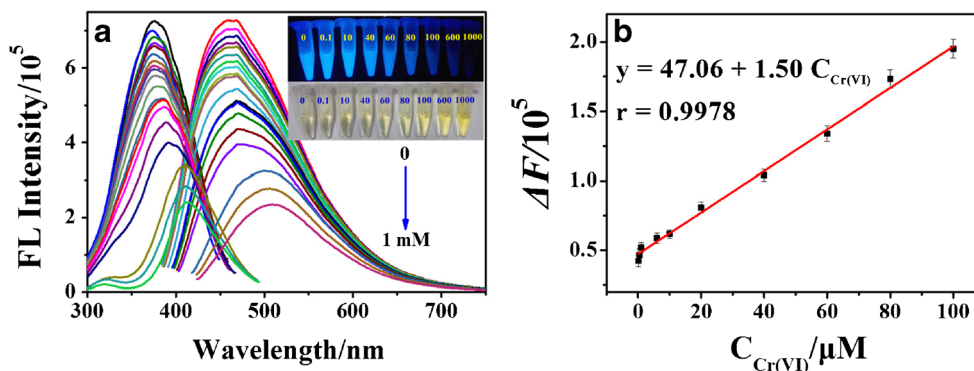
Quenching mechanism study of Cr(VI) on the IrNCs

Fluorescence quenching is the fluorescence intensity decrease of fluorophore by various interactions with quenchers, including excited-state reactions, molecular rearrangements, energy transfer, ground-state complex formation, and collisional quenching [13]. In the presence of Cr(VI), the fluorescence of the IrNCs is quenched and the excitation and emission spectra occur red-shift (**Fig. 4a**). This contributes to the changed microstructure of the IrNCs under the oxidation of Cr(VI). The absorbance spectra of IrNCs is entirely different in the presence and absence of Cr(VI), suggesting one nonfluorescent ground-state complex formation between IrNCs and Cr(VI) (**Fig. 4b**). The fluorescence quenching mode was also investigated according to the Stern-Volmer equation $F_0/F = 1 + K_q\tau_0[Q] = 1 + K_{sv}[Q]$, where F and F_0 stand for fluorescence intensities in the presence and absence of the quencher, respectively, τ_0 is the lifetime of the fluorophore in the absence of quencher, $[Q]$ is the concentration of the quencher, K_q and K_{sv} are the quenching rate constant and Stern-Volmer quenching constant, respectively. **Fig. 4c** depicts the Stern-Volmer plots of the fluorescence of IrNCs quenched by the Cr(VI) and **Table 1** shows the K_q and K_{sv} under different reaction temperature. With the increasing of the reaction temperature, the K_q and K_{sv} decline, suggesting that the increased

Table 1 Stern-Volmer constant of interaction between the IrNCs and Cr(VI) at different temperatures (r : correlation coefficient of the Stern-Volmer equations)

| T/K | $K_{sv} (\text{L}\cdot\text{mol}^{-1})$ | $K_q (\text{L}\cdot\text{mol}^{-1}\cdot\text{s}^{-1})$ | r |
|--------------|---|--|--------|
| 298.15 K | 4.98×10^3 | 2.2751×10^{12} | 0.9961 |
| 308.15 K | 4.48×10^3 | 2.0267×10^{12} | 0.9950 |
| 318.15 K | 4.05×10^3 | 1.8502×10^{12} | 0.9975 |

Fig. 5 **a** The fluorescence spectra of the IrNCs in the presence of different Cr(VI) concentration in pH 3.0 acetate buffer, inset: the corresponding photographs under visible light and 365 nm UV lamp; **b** Linear relationship between the ΔF with Cr(VI) concentration in range of 0.1 to 100 μM under room temperature



reaction temperature accelerates the formation of ground-state complex. This complex absorbs light and immediately returns to the ground state without emission of a photon. Moreover, the introduction of Cr(VI) can not change the fluorescence lifetime of the IrNCs (**Fig. S3**). These results confirmed that the quenching mode of Cr(VI) to the IrNCs can be ascribed as static quenching.

Determination of Cr(VI)

Cr(VI) is one of main pollution in soils and waters due to its wide use in leather tanning, textile industries, electroplating, metal finishing, nuclear power plant, and chromate preparation [29]. Owing to the high oxidizing potential and permeability of biological membranes, it has been considered to be hazardous to human beings and have potent carcinogenic and mutagenic effects [30]. World Health Organization (WHO) and the United States Environmental Protection Agency (EPA) state the maximum tolerant chromium concentration in drinking water are 0.96 and 0.19 μM [31, 32]. Thus, the rapid determination of trace Cr(VI) in water is very significant. It has been found that the strong fluorescence of the IrNCs can be quenched in the presence of Cr(VI) and the excitation and emission spectra have an obvious redshift (**Fig. 5a**). The fluorescence intensity of the IrNCs decreases proportionately with the increasing concentration of Cr(VI) from 0.1 to 100 μM (**Fig. 5b**). The regression equation was $\Delta F = 47.06 + 1.50 C_{\text{Cr(VI)}}$ with the correlation coefficient (r) of 0.9987, and the detection limit

was calculated to be 0.025 μM (calculated by $3S_b/k$, hereinto, $3S_b/k$ referred to the quotient between triple of the blank reagent's standard deviation and the slope of the working curve; S_b referred to the standard deviation of 11 parallel analysis of the blank reagent. S_b is 4.9%, k is the slope of the working curve). The determination result is lower than the WHO and EPA standard. The color of the IrNCs changes from colorless to faint yellow with the increasing gradually of Cr(VI) under visible light, while the fluorescence intensity of IrNCs gradually was quenched irradiating by 365 nm UV light (**Fig. 5a** inset).

Fluorometric methods based on various nanomaterials for the determination of Cr(VI) are compared in **Table 2**. The determination limit and linear range of this work are comparable with fluorescent CuNCs, CdTe quantum dots and Silicon nanoparticles [14, 33–35]. The preparation conditions of the IrNCs are gentler than CdTe quantum dots and Silicon nanoparticles [33, 34]. The excellent stability and potential environmental safety endow IrNCs with superiority over other fluorescent nanomaterials [16]. Thus, the fluorescent IrNCs show the great application promising in many analytical chemistry fields.

The selectivity of this fluorescent method for Cr(VI) determination was assessed by investigating the effects of frequently encountered interferences. Anions, such as $\text{P}_2\text{O}_7^{4-}$, I^- , $\text{S}_2\text{O}_8^{2-}$, F^- , ClO_4^- , Br^- , IO_3^- , HSO_4^- , $\text{S}_2\text{O}_3^{2-}$, NO_2^{2-} , CO_3^{2-} , NO_3^- , BrO_3^- and IO_4^- , biomolecules, including melamine, BSA, cysteine, uric acid, Vc, glutathione, ovalbumin, 3-hydroxytyramine hydrochloride, L-lysine, L(+)-arginine, L-tryptophane, L-tyrosine, L-

Table 2 Comparison of the analytical performances of different methods for the determination of Cr(VI)

| Methods | Materials used | Linear range/ μM | LODs/ nM | Refs. |
|--------------|-----------------------|-----------------------------|----------|-------------|
| Fluorescence | IrNCs | 0.1 to 100 | 25 | This method |
| Fluorescence | CuNCs | 0.2–60 | 65 | [14] |
| Fluorescence | CdTe quantum dots | 0.2–20 | 154 | [33] |
| Fluorescence | Silicon nanoparticles | 0.1–200 | 28 | [34] |
| Fluorescence | Carbon dots | 1–10 | 200 | [35] |
| Fluorescence | Graphene quantum dots | 0.05–500 | 3.7 | [16] |

Table 3 Concentration determination of Cr(VI) in the water samples

| Samples | Added (μM) | Found (μM) | RSD (%) | Recovery (%) |
|------------|-------------------------|-------------------------|---------|--------------|
| Tap water | 0 | 0 | – | – |
| | 50 | 48.7 | 2.3 | 97.4 |
| | 30 | 30.2 | 4.0 | 100.6 |
| | 20 | 20.3 | 3.1 | 101.5 |
| Lake water | 0 | 0 | – | – |
| | 50 | 51.2 | 4.3 | 102.4 |
| | 30 | 30.7 | 2.8 | 102.3 |
| | 20 | 19.9 | 3.6 | 99.5 |
| Seawater | 0 | 0 | – | – |
| | 50 | 49.7 | 3.8 | 99.4 |
| | 30 | 30.1 | 4.1 | 100.3 |
| | 20 | 19.5 | 2.7 | 103.5 |

phenylalanine, L-proline, L-methionine and L-glutamic acid have no obvious influence to the determination of Cr(VI) (Fig. S6, 7). Other ions do not disturb the analysis of Cr(VI) except for a minor effect caused by MnO_4 in concentrations of $>50 \mu\text{M}$ (Fig. S8). These results show the high selectivity of IrNCs fluorescence sensor for Cr(VI) determination.

Sample analysis

The Cr(VI) concentration in tap water, lake and seawater were determined to test the applicability of this method. Different dosage of Cr(VI) was added to the sample matrices to determine recovery. In Table 3, the RSD (three parallel determinations) and recovery are calculated based on the concentration determination of Cr(VI) added. The RSD was less than $\pm 5\%$ and the recovery was 97.4–103.5%, suggesting good accuracy of this method.

Conclusions

Fluorescent IrNCs consisting of 2–7 Ir atoms were prepared in DMF solution. The average size is about $0.9 \pm 0.2 \text{ nm}$ and fluorescence lifetime is about 2.2 ns. These novel IrNCs emit strong bluish green light and exhibit excitation wavelength-dependent emission. Their quantum yield is calculated to be 8.3% which is unsatisfactory and need to be improved. The IrNCs show excellent solubility in water, ethanol and DMF, and the fluorescence spectra are different in different solvents depending on the solvent polarity and local environment. Based on the static quenching action of Cr(VI), the IrNCs can be used for the determination of Cr(VI). The easy preparation and attractive fluorescence of the IrNCs suggest a further exploration on this nanomaterial.

Acknowledgements This work was supported by the National Natural Science Foundation of China (No. 51502115), and the 111 Project (B13025).

Compliance with ethical standards The author(s) declare that they have no competing interests.

References

1. Tanaka SI, Miyazaki J, Tiwari DK, Jin T, Inouye Y (2011) Fluorescent platinum nanoclusters: synthesis, purification, characterization, and application to bioimaging. *Angew Chem* 123:451–455
2. ZK W, Jin RC (2010) On the ligand's role in the fluorescence of gold nanoclusters. *Nano Lett* 10:2568–2573
3. Yahia-Ammar A, Sierra D, Mérola F, Hildebrandt N, Guével XL (2016) Self-assembled gold nanoclusters for bright fluorescence imaging and enhanced drug delivery. *ACS Nano* 10:2591–2599
4. Nair LV, Nazeer SS, Jayasree RS, Ajayaghosh A (2015) Fluorescence imaging assisted photodynamic therapy using photosensitizer-linked gold quantum clusters. *ACS Nano* 7: 5825–5832
5. Yuan ZQ, Cai N, Du Y, He Y, Yeung ES (2014) Sensitive and selective detection of copper ions with highly stable polyethyleneimine-protected silver nanoclusters. *Anal Chem* 86: 419–426
6. Liu MM, Chen W (2013) Green synthesis of silver nanoclusters supported on carbon nanodots: enhanced photoluminescence and high catalytic activity for oxygen reduction reaction. *Nano* 5: 12558–12564
7. Xie JP, Zheng YG, Ying JY (2009) Protein-directed synthesis of highly fluorescent gold nanoclusters. *J Am Chem Soc* 131:888–889
8. Yuan X, Yao QF, Yu Y, Luo ZT, Xie JP (2014) Novel synthetic strategies for thiolate-protected Au and Ag nanoclusters: towards atomic precision and strong luminescence. *RSC Smart Materials* 7: 131–168
9. Chen WH, Shen QT, Bartynski RA, Kaghazchi P, Jacob T (2013) Reduction of nitric oxide by acetylene on Ir surfaces with different morphologies: comparison with reduction of NO by CO. *Langmuir* 29(4):1113–1121
10. Vankayala R, Gollavelli G, Mandal BK (2013) Highly fluorescent and biocompatible iridium nanoclusters for cellular imaging. *J Mater Sci Mater Med* 24:1993–2000
11. Bhat S, Chakraborty I, Maark TA, Mitra A, De G, Pradeep T (2016) Atomically precise and monolayer protected iridium clusters in solution. *RSC Adv* 6:26679–26688
12. Oikawa K, Itoh S, Yano H, Kawasaki H, Obora Y (2017) Preparation and use of DMF-stabilized iridium nanoclusters as methylation catalysts using methanol as the C1 source. *Chem Commun* 53:1080–1083
13. Lakowicz JR (2006) Principles of fluorescence spectroscopy. Springer, New York, pp 7–9
14. Cui ML, Song G, Wang C, Song QJ (2015) Synthesis of cysteine-functionalized water-soluble luminescent copper nanoclusters and their application to the determination of chromium(VI). *Microchim Acta* 182:1371–1377
15. Würth C, Grabolle M, Pauli J, Spieles M, Resch-Genger U (2013) Relative and absolute determination of fluorescence quantum yields of transparent samples. *Nat protoc* 8(8):1535–1550
16. Huang S, Qiu HN, Zhu FW, SY L, Xiao Q (2015) Graphene quantum dots as on-off-on fluorescent probes for chromium(VI) and ascorbic acid. *Microchim Acta* 182:1723–1731

17. Liu Q, Guo BD, Rao ZY, Zhang BH, Gong JR (2013) Strong two-photon-induced fluorescence from photostable, biocompatible nitrogen-doped graphene quantum dots for cellular and deep-tissue imaging. *Nano Lett* 13:2436–2441
18. Zhang YW, Peng HS, Huang W, Zhou YF, Yan DY (2008) Facile preparation and characterization of highly antimicrobial colloid Ag or Au nanoparticles. *J Colloid Interface Sci* 325:371–376
19. Chen HJ, Wang YL, Wang YZ, Dong SJ, Wang EK (2006) One-step preparation and characterization of PDDA-protected gold nanoparticles. *Polymer* 47:763–766
20. Zhao L, Jin Y, Yan ZW, Liu YY, Zhu HJ (2012) Novel, highly selective detection of Cr(III) in aqueous solution based on a gold nanoparticles colorimetric assay and its application for determining Cr(VI). *Anal Chim Acta* 731:75–81
21. Ortiz R, Cuesta A, Márquez OP, Márquez J, Méndez JA (1999) Gutiérrez C (1999) origin of the infrared reflectance increase produced by the adsorption of CO on particulate metals deposited on moderately reflecting substrates. *J Electroanal Chem* 465:234–238
22. Frank M, Bäumer M (2000) From atoms to crystallites: adsorption on oxide-supported metal particles. *Phys Chem Chem Phys* 2: 3723–3737
23. Cui ML, Zhou JD, Zhao Y, Song QJ (2017) Facile synthesis of iridium nanoparticles with superior peroxidase-like activity for colorimetric determination of H₂O₂ and xanthine. *Sensors Actuators B Chem* 243:203–210
24. Xian JY, Hua Q, Jiang ZQ, Ma YS, Huang WX (2012) Size-dependent interaction of the poly(N-vinyl-2-pyrrolidone) capping ligand with Pd nanocrystals. *Langmuir* 28:6736–6741
25. Wen XM, Yu P, Toh YR, Ma XQ, Huang SJ, Tang J (2013) Fluorescence origin and spectral broadening mechanism in atomically precise Au₈ nanoclusters. *Nano* 5:10251–10257
26. Díez I, Ras RHA, Kanyuk MI, Demchenko AP (2013) On heterogeneity in fluorescent few-atom silver nanoclusters. *Phys Chem Chem Phys* 15:979–985
27. Demchenko AP (2008) Site-selective red-edge effects. *Methods Enzymol* 450:59–78
28. SN Q, Chen H, Zheng XM, Cao JS, Liu XY (2013) Ratiometric fluorescent nanosensor based on water soluble carbon nanodots with multiple sensing capacities. *Nano* 5:5514–5518
29. Zhang JR, Zeng AL, Luo HQ, Li NB (2016) Fluorescent silver nanoclusters for ultrasensitive determination of chromium(VI) in aqueous solution. *J Hazard Mater* 304:66–72
30. Kotas J, Stasicka Z (2000) Chromium occurrence in the environment and methods of its speciation. *Environ Pollut* 107:263–283
31. California Department of Public Health. Chromium-6 in drinking water: regulation update, <http://ww2.cdph.ca.gov/CERTLIC/DRINKINGWATER/Pages/Chromium6.aspx>
32. United States Environmental Protection Agency. List of drinking water contaminants & MCLs, EPA, 816-F-03-016, <http://www.epa.gov/safewater/contaminants/index.html#listmcl>
33. Zhang LJ, CL X, Li BX (2009) Simple and sensitive detection method for chromium(VI) in water using glutathione-capped CdTe quantum dots as fluorescent probes. *Microchim Acta* 166:61–68
34. Zhu LJ, Peng X, Li HT, Zhang YY, Yao SZ (2017) On-off-on fluorescent silicon nanoparticles for recognition of chromium(VI) and hydrogen sulfide based on the inner filter effect. *Sensors Actuators B Chem* 238:196–203
35. Zhang HQ, Huang YH, ZB H, Tong CQ, Zhang ZS, SR H (2017) Carbon dots codoped with nitrogen and sulfur are viable fluorescent probes for chromium(VI). *Microchim Acta* 184:1547–1553